ELSEVIER

Computational Materials Science 19 (2000) 292–297

COMPUTATIONAL MATERIALS SCIENCE

www.elsevier.com/locate/commatsci

An FE-analysis of anisotropic creep damage and deformation in the single crystal SRR99 under multiaxial loads

W. Qi [a,*], W. Brocks [a], A. Bertram [b]

[a] *Institute for Materials Research, GKSS Research Center, D-21502 Geesthacht, Germany*
[b] *Institut für Mechanik, Otto-von-Guericke-Universität, D-39016 Magdeburg, Germany*

Abstract

Multidimensional stress–strain and damage analyses of engineering structural components with the help of numerical simulations are of great interest. These can only be done by using adequate material models and suitable numerical methods. Bertram and Olschewski (Computational modelling of anisotropic materials under creep conditions, Math. Modelling Sci. Comp. 5 (1995) 100–109; Anisotropic creep modeling of the single crystal superalloy SRR99, J. Comp. Mater. Sci. 5 (1996) 12–16), proposed a three-dimensional creep model for single crystals. An anisotropic creep damage model for single crystals was also suggested by Qi and Bertram (W. Qi, A. Bertram, Anisotropic creep damage modeling of single crystal superalloys, Tech. Mech. 17 (1997) 313–322; W. Qi, Modellierung der Kriechschadigung einkristalliner Superlegierungen in Hochtemperaturbereich, Ph.D. dissertation, Technical University Berlin, VDI Verlag, Düsseldorf, 1998; W. Qi, A. Bertram, Damage modeling of the single crystal superalloy SRR99 under monotonous creep, Comput. Mater. Sci. 13 (1998) 132–141). The coupled model has been used to predict the creep deformation and the lifetime of the single crystal SRR99 under uniaxial creep loads at 760°C. The purpose of this work is the application of the coupled model to the simulation of multiaxial creep behavior and damage development, and its dependence upon non-proportional loading paths of SRR99 at 760°C.

Keywords: Single crystal superalloy; Anisotropic damage; Finite-element method; Multiaxial creep

1. Introduction

The thermomechanical loading applied to gas turbine blades is complex and multiaxial. Computational modeling tools are being developed to optimize the design and to predict the lifetime of such hot-section components. The strong requirements in design procedures (safety, reliability) involve the development of sophisticated lifetime prediction techniques, taking into account the anisotropic damage evolution under multiaxial and non-proportional loading conditions. A phenomenological multiaxial creep model for studying the primary and secondary creep behavior of materials with cubic symmetry was developed by Bertram and Olschewski [1,2]. However, the material damage has not been considered in this model. Based on continuum damage mechanics (CDM) [3,4], Qi and Bertram proposed an anisotropic damage model [5–7]. By coupling both models according to the effective stress concept of

* Corresponding author. Tel.: +49-4152-872552; fax: +49-4152-872595.
E-mail address: weidong.qi@gkss.de (W. Qi).

0927-0256/00/$ - see front matter
PII: S0927-0256(00)00166-X

CDM, the original creep model can be extended to simulate the tertiary creep behavior and to predict creep rupture. In previous works the authors reported the process of identification of the material parameters by uniaxial tensile creep tests [1,2,6], and the results of the simulation of the uniaxial creep behavior of Ni-based single crystal superalloys SRR99 [7] and CMSX-6 [8] at 760°C. The results show that both the influence of material symmetry on creep behavior and the non-linearity of material response with respect to the applied loads are reproduced by the proposed model.

However, the capability of this model, especially for the case of multidimensional non-proportional loading conditions, has not been investigated in the previous works. This paper reports the results of further studies related to this aspect and focuses on the theoretical investigations on how damage develops under multidimensional loads and how the changing of the load path influences damage development.

Prediction of creep lifetime consists of the analysis of the inelastic strains in the most critical areas of the structure, often in a region of stress concentration. In gas turbine blades with cooling design, the typical stress concentration occurs due to the air cooling channels. For this reason we choose a square plate with a circular hole in the middle, as a sample representation of the area of blades where the air cooling channels appear. As we only consider tensile creep loading conditions in this work, the passive damage effect is neglected to save computer time. The numerical calculation was carried out by the commercial finite-element code ABAQUS by implementing the proposed model into the user-supplied material model.

2. Summary of the constitutive equations

The development of the models and the identification of the material parameters at 760°C are described in the previous works [1,2,6,7]. Here we just give a brief summary of the constitutive equations without considering the passive damage.

The creep model coupled with damage is expressed as follows:

$$\dot{\boldsymbol{\varepsilon}} = \overset{\langle 4\rangle}{\mathbf{A}}_1 : \dot{\tilde{\boldsymbol{\sigma}}} + \overset{\langle 4\rangle}{\mathbf{A}}_2 : \tilde{\boldsymbol{\sigma}} + \overset{\langle 4\rangle}{\mathbf{A}}_3 : \boldsymbol{\tau}, \tag{1}$$

$$\dot{\boldsymbol{\tau}} = \overset{\langle 4\rangle}{\mathbf{A}}_4 : \dot{\tilde{\boldsymbol{\sigma}}} + \overset{\langle 4\rangle}{\mathbf{A}}_5 : (\tilde{\boldsymbol{\sigma}} - \boldsymbol{\tau}), \tag{2}$$

where $\boldsymbol{\varepsilon}$, $\tilde{\boldsymbol{\sigma}}$ and $\boldsymbol{\tau}$ are the strain tensor, the effective stress tensor, and a tensorial internal variable of rank two, respectively, and $\overset{\langle 4\rangle}{\mathbf{A}}_j$ $(j = 1,2,3,4,5)$ are fourth-order material tensors.

The effective stress tensor is defined by

$$\tilde{\boldsymbol{\sigma}} = (\mathbf{I} - \mathbf{D})^{-1/2} \cdot \boldsymbol{\sigma} \cdot (\mathbf{I} - \mathbf{D}^{\mathrm{T}})^{-1/2}, \tag{3}$$

where $\mathbf{D}$ is the second-order damage tensor, and $\mathbf{I}$ denotes the identity tensor. The damage evolution law is given as:

$$\dot{\mathbf{D}} = \left(\alpha_1 \mathbf{I} \otimes \mathbf{I} + \alpha_2 \overset{\langle 4\rangle}{\mathbf{I}} + \alpha_3 \overset{\langle 4\rangle}{\mathbf{R}}\right) : \sum_{i=1}^{3} \left\langle \frac{\eta_i \hat{\sigma}_i}{B} \right\rangle^n \hat{\mathbf{n}}_i^{\sigma} \otimes \hat{\mathbf{n}}_i^{\sigma}, \tag{4}$$

with

$$\overset{\langle 4\rangle}{\mathbf{R}} = \sum_{i=1}^{3} \mathbf{e}_i^k \otimes \mathbf{e}_i^k \otimes \mathbf{e}_i^k \otimes \mathbf{e}_i^k, \tag{5}$$

and the damage active stress tensor $\hat{\boldsymbol{\sigma}}$ and the orientation function η_i defined as follows:

$$\hat{\boldsymbol{\sigma}} = (\mathbf{I} - \mathbf{D})^{-p} \cdot \boldsymbol{\sigma} \cdot (\mathbf{I} - \mathbf{D}^{\mathrm{T}})^{-p} = \sum_{i=1}^{3} \hat{\sigma}_i \hat{\mathbf{n}}_i^{\sigma} \otimes \hat{\mathbf{n}}_i^{\sigma}, \tag{6}$$

$$\eta_i = \left[\sum_{j=1}^{3} (\hat{\mathbf{n}}_i^{\sigma} \cdot \mathbf{e}_j^k)^{2m}\right]^q = \left[(\hat{\mathbf{n}}_i^{\sigma} \cdot \mathbf{e}_1^k)^{2m} + (\hat{\mathbf{n}}_i^{\sigma} \cdot \mathbf{e}_2^k)^{2m} + (\hat{\mathbf{n}}_i^{\sigma} \cdot \mathbf{e}_3^k)^{2m}\right]^q, \tag{7}$$

where $\overset{\langle 4\rangle}{\mathbf{I}}$ denotes the fourth-order identity tensor and $\mathbf{e}_j^k$ $(j = 1,2,3)$ are the lattice vectors.

It is assumed that rupture takes place when the maximum principal value of the damage tensor is equal to a critical value D_{R}. For SRR99 at 760°C this value has been obtained from the uniaxial tensile creep tests as 0.2. However, for the visco-plastic FE-calculation of structural components, the principal values of the damage tensor at a certain integration point can be greater than D_{R}.

3. Finite-element calculation

The above constitutive equations have been implemented into the commercial finite-element code ABAQUS as the user-supplied material subroutine UMAT [9]. The explicit integration method of Euler has been used for the numerical integration. The length and the thickness of the square plate are 10.0 and 0.2 mm, respectively, and the radius of the hole is 0.5 mm. Fig. 1 shows the FE-mesh used for the calculations and the applied loading conditions. The three-dimensional eight-node linear brick hybrid continuum element, C3D8H, of the element library of ABAQUS is used for all calculations presented in this work.

In order to get a clear understanding of how the lattice orientation effects the damage and the deformation behavior, we simply consider the situation when the Eulerian angle, φ_2, between the [0 0 1]-direction and the longitudinal axis of the blade changes, while the Eulerian angles φ_1 and φ_3 are kept equal to zero. Two cases are studied: (a) $\varphi_2 = 0°$, which corresponds to the perfectly cast blade, and (b) $\varphi_2 = 10°$. Needless to say, the influence of the angles φ_1 and φ_3 is also of importance, but their variation would greatly increase the difficulty of presentation of the results.

The loading process consists of two stages, as illustrated in Fig. 2. During the first phase of 10 h, the plate is subject to a constant load of $\sigma_3 = 180$ MPa in the 3-direction. In the second phase, an additional creep load of $\sigma_2 = 180$ MPa in the 2-direction is applied, so that by this time the plate is subject to a two-dimensional tensile load. Note that the stress state at the cold inner surface of a blade is approximately bi-axial tension.

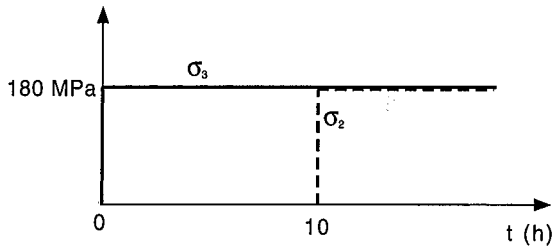

Fig. 2. Loading process.

4. Results and discussion

4.1. Case (a): $\varphi_2 = 0°$

In the first loading phase, the plate is subject to a distributed constant tensile load σ_3 in the 3-direction. Fig. 3 shows the distribution of the maximum principal stress immediately after the load is imposed. The stress concentration at the hole is clearly seen in the figure. The maximum tensile stress reaches a value of above 460 MPa in the [0 0 1]-direction, and a value of about 260 MPa in the [0 1 1]-direction. As the evolution rate of the creep damage depends not only on the level of the applied stress but also on its direction, the damage

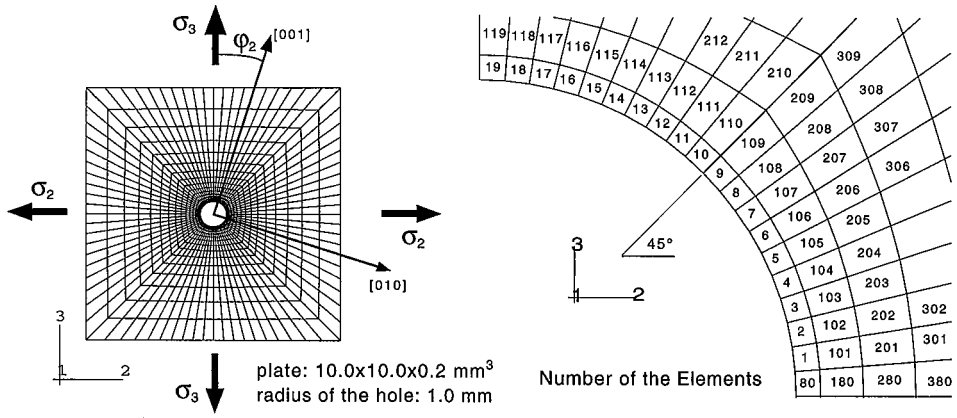

Fig. 1. Finite-element mesh and loading condition.

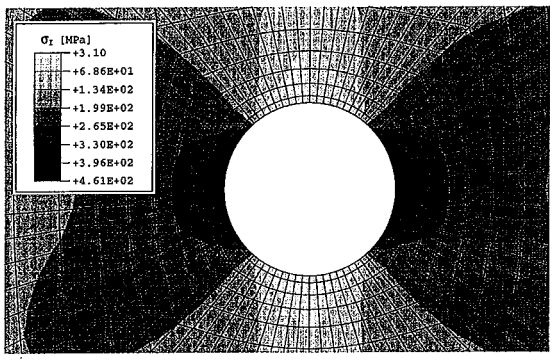

Fig. 3. Distribution of the maximum principal stress at $t = 0.001$ h, Case (a).

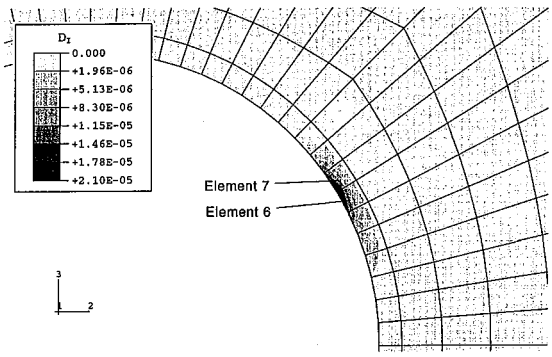

Fig. 4. Distribution of the maximum principal damage at $t = 9.8$ h, Case (a).

does not always develop most quickly at the area where the maximum stress occurs. Fig. 4 shows the damage state at the time $t = 9.8$ h, before the second loading phase begins. It can be seen that the elements 6 and 7 suffer the maximum damage at that time. After the second load σ_2 has been applied, a strong redistribution of the stresses takes place. A contour plot of the maximum principal stress at the time $t = 10.8$ h is shown in Fig. 5. Now the maximum tensile stress occurs in the elements 9 and 10, and the corresponding principal direction coincides with the [0 1 1]-direction. Henceforth, needless to say, the damage will develop most quickly in these elements. Figs. 6(a) and (b) show the contour plot of the maximum principal value of the damage and of the strain tensor at the time $t = 80$ h, respectively. The maximum principal damage in the elements 9 and 10 partly reaches the

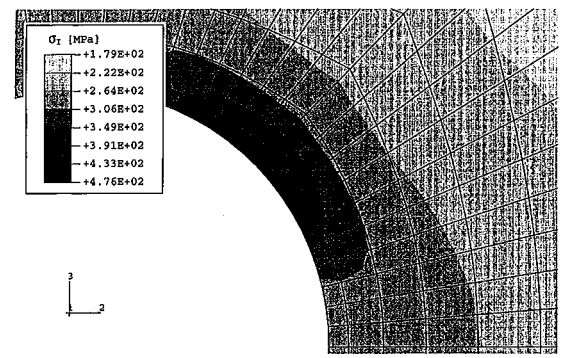

Fig. 5. Distribution of the maximum principal stress at $t = 10.8$ h, Case (a).

critical value $D_R = 0.2$. The maximum strain, however, is only 0.303% at this time.

4.2. Case (b): $\varphi_2 = 10°$

As for Case (a), the corresponding stress, damage and strain distributions of Case (b) at times $t = 0.001$, 9.88, 10.3 and 48.6 h are shown in Figs. 7–10(a), (b), respectively. The maximum principal stress at time $t = 0.001$ h reaches a value of 558 MPa, almost 100 MPa more than in Case (a). Comparing Figs. 4 and 8 we will find that in Case (b) the damage develops more quickly than in Case (a). The distribution of the maximum principal stress at $t = 10.3$ h is similar to that of Case (a). The damage develops generally faster than in Case (a). After ca. 49 h, two elements are totally damaged (see Fig. 10(a)), and the damage and strain states are similar to those at $t = 80$ h in Case (a).

5. Concluding remarks

As a continuation of the previous works, this paper presents the results of numerical analyses of damage development and deformation behavior of a square plate with a hole, which is made of the single crystal superalloy SRR99 and subject to non-proportional two-dimensional creep loads. From this study we get the following results. First, the stress concentration near the hole leads to a rapid development of damage and to local failure.

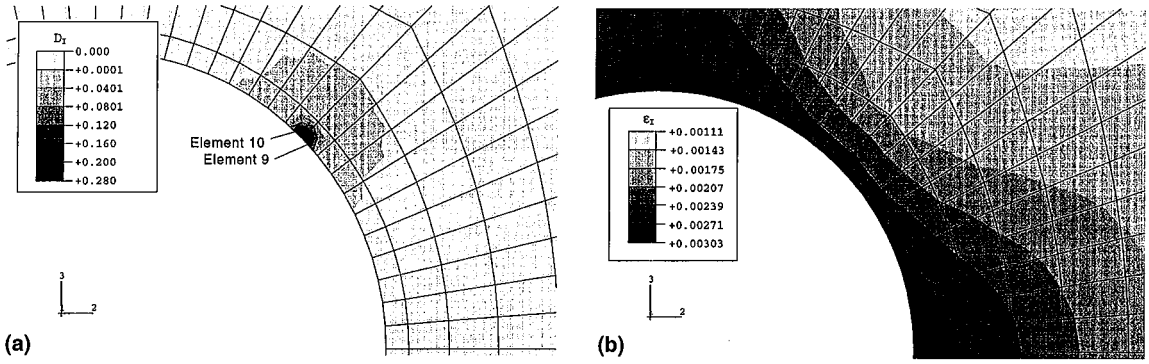

Fig. 6. Distribution of the maximum principal damage (a), and strain (b) at $t = 80$ h, Case (a).

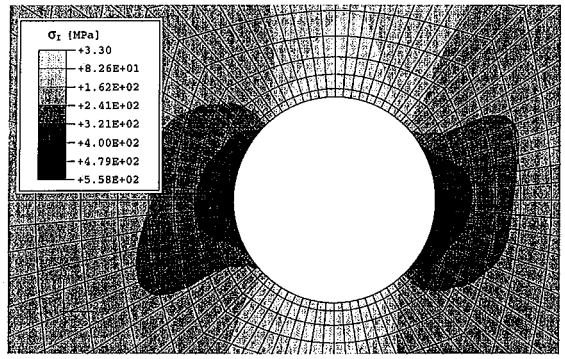

Fig. 7. Distribution of the maximum principal stress at $t = 0.001$ h, Case (b).

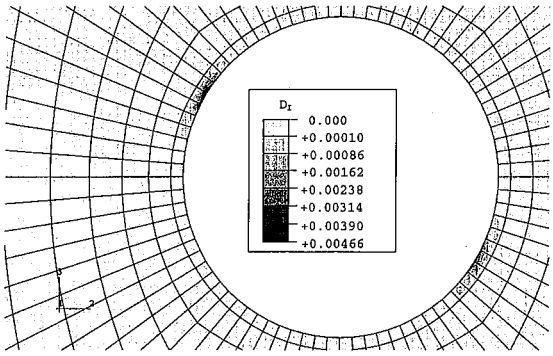

Fig. 8. Distribution of the maximum principal damage at $t = 9.88$ h, Case (b).

Second, although local damage reaches the critical values and local failure takes place, the inelastic strain can be still under the design limit. Third, the

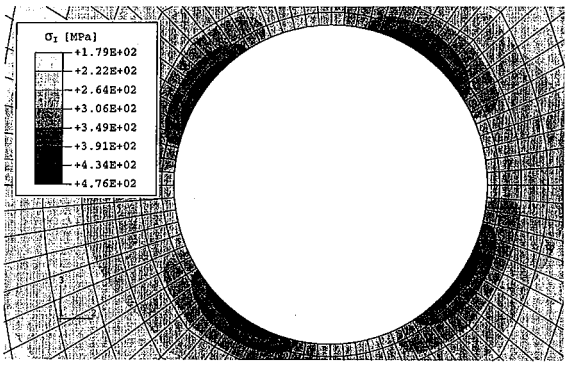

Fig. 9. Distribution of the maximum principal stress at $t = 10.3$ h, Case (b).

effect of lattice orientation on damage behavior is remarkable.

The average inelastic strain of gas turbine blades is designed to be less than about 1–2%. However, although the permitted inelastic deformation of such high-temperature structural components is limited, the local strain may reach a much greater value than the average one, which will lead to stress redistribution and local failure. Moreover, as the above study shows, local failure can take place without large inelastic strains. Experimental results of Ni-based single crystal superalloys also show that there is hardly a secondary creep period when the applied creep stress is above a certain level at a given temperature; the creep curve directly goes from the primary to the tertiary period. Therefore, the use of advanced material models, which take into ac-

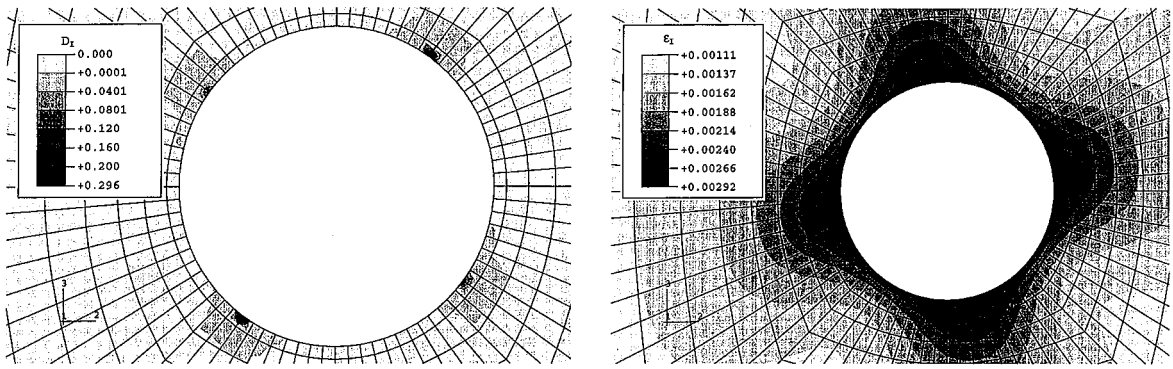

Fig. 10. Distribution of the maximum principal damage (a), and strain (b) at $t = 48.6$ h, Case (b).

count damage and tertiary creep behavior, is necessary in modern design.

References

[1] A. Bertram, J. Olschewski, Computational modelling of anisotropic materials under creep conditions, Math. Modelling Sci. Comput. 5 (1995) 100–109.

[2] A. Bertram, J. Olschewski, Anisotropic creep modeling of the single crystal superalloy SRR99, J. Comp. Mat. Sci. 5 (1996) 12–16.

[3] J.L. Chaboche, Continuum damage mechanics: part I – general concepts; part II – damage growth, crack initiation, J. Appl. Mech. 55 (1998) 59–72.

[4] D. Krajcinovic, Damage Mechanics, Elsevier, Amsterdam, 1996.

[5] W. Qi, A. Bertram, Anisotropic creep damage modeling of single crystal superalloys, Tech. Mech. 17 (1997) 313–322.

[6] W. Qi, Modellierung der Kriechschädigung einkristalliner Superlegierungen im Hochtemperaturbereich, Ph. D. dissertation, Technical University Berlin, VDI Verlag, Düsseldorf, 1998.

[7] W. Qi, A. Bertram, Damage modeling of the single crystal superalloy SRR99 under monotonous creep, Comput. Mater. Sci. 13 (1998) 132–141.

[8] W. Qi, A. Bertram, Anisotropic continuum damage modeling for single crystals at high temperatures, Int. J. Plasticity 15 (1999) 1197–1215.

[9] ABAQUS Standard, Version 5.8, Theory Manual, Hibbit, Karlsson and Sorensen, Inc., Pawtucket, RI, USA, 1998.